International Journal of Adhesion & Adhesives 130 (2024) 103619

Contents lists available at ScienceDirect

International Journal of Adhesion and Adhesives

journal homepage: www.elsevier.com/locate/ijadhadh

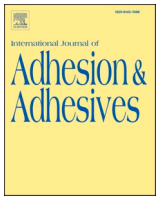

Modelling the static and fatigue behavior of hybrid spot welded-adhesively bonded single lap joints

Sajjad Safaei, Luca Michele Martulli, Andrea Bernasconi *, Michele Carboni

Department of Mechanical Engineering, Politecnico di Milano, Via La Masa 1, Milano, 20156, Italy

ARTICLE INFO

Keywords:
Hybrid joints
Ultrasonically spot-welded joints
Adhesively bonded joints
Single lap joints
Static strength
Fatigue strength
Virtual Crack Closure Technique
Load ratio

ABSTRACT

Hybrid joints formed by combining two or more joining methods, including spot welding and adhesive bonding, are relatively new joints designed especially for use in the automotive industry. The aim of this work is to study numerically the static and fatigue behavior of ultrasonically spot-welded, adhesively bonded and hybrid spot welded – adhesive bonded joints. The Virtual Crack Closure Technique was used to model the experimental static and fatigue tests for single lap joints reported in the literature. By introducing a short fictitious initial crack, in static loading the simulations matched the experimental results, characterized by a higher stiffness and static strength of the bonded and hybrid joints compared to the just spot-welded ones, and by an approximately similar static strength of the bonded and the hybrid joints. By the same method, a good match between the numerical and the experimental fatigue strengths was found, with the hybrid joints providing higher strength compared to the just spot-welded joints at 0.1 load ratio. According to the numerical analyses, S–N curves of bonded joints are expected to be statistically similar to those of the hybrid joints. This indicates that the adhesive plays the major role in the fatigue behaviour of the hybrid joint. Finally, the fatigue strength of hybrid joints was simulated at 0.3 load ratio. It was found a reasonable agreement between the experimental and numerical observations at 0.3 load ratio. The VCCT proved to be capable of simulating the static and the fatigue behaviour of the hybrid joints, thus proving to be a tool useful for the interpretation of the results and for the design of other hybrid joint configurations.

1. Introduction

Joining of parts is usually done by mechanical fastening, welding or adhesive bonding. Among welding procedures, Ultrasonic Spot Metal Welding (USMW) technique has recently become interesting for some specific technical applications [1]. This technique needs low energy, and it is based on a solid-state plastic deformation that results in a reasonably homogenous microstructure between the base joined materials [2]. Also, USMW technology can be quick and efficient. However, spot-welded joints have major disadvantages such as high stress concentration, low static and fatigue strength and low fatigue life [3–7]. The use of adhesives as a bonding technology has been increasing in the last decades. Bonded joints are used in numerous fields such as aerospace, aeronautical, automotive, civil engineering, and sports equipment. Compared with ultrasonic spot welding joints, adhesively bonded joints have a larger strength-to-weight ratio [8,9]. Also, they offer a more uniform stress distribution, higher fatigue strength and a superior stiffness [10,11]. However, near the overlapping edges, the adhesive-bonded substrates stretch considerably, so the shear stress is not uniform and shows local peak stresses resulting in the failure of bonded joints, especially for brittle adhesives [12,13]. In addition, adhesively bonded joints are sensitive to temperature, humidity, ageing and surface treatment [14–16].

Hybrid welded-bonded joints have been recently used to improve the static and fatigue performance of spot-welded joints [17,18]. Also, hybrid spot welded-bonded joints are easier to be manufactured with respect to adhesive ones, since the spot weld keeps in position the adherends, so handling time is shortened. Hybrid joints are usually obtained by merging any two-joining technology such as rivet-bonded, clinch-adhesive, bolted-bonded and weld-adhesive [18–24]. Hybrid joints improve the static and fatigue properties by significantly increasing load transfer in the inner overlap zones [25–28]. Souza et al. [27] used cohesive zone model (CZM) to predict numerically the mechanical performance of the single lap bonded, resistance spot-welded and hybrid joints in static loading condition. Based on the results, it was observed that the stiffness of the hybrid joint is 93% greater than

* Corresponding author.
E-mail address: andrea.bernasconi@polimi.it (A. Bernasconi).

https://doi.org/10.1016/j.ijadhadh.2024.103619
Received 31 July 2023; Received in revised form 29 September 2023; Accepted 2 January 2024
Available online 3 January 2024

that of the resistance spot-welded joint. Costa et al. [28], Moroni et al. [18] and Sadowski et al. [29] have compared the mechanical response of the single lap resistance spot welded-bonded specimens with the single lap resistance spot-welded joints subjected to the static loading. They found that the static strength of the single lap joints is improved with the use of hybrid joints. Pizzorni et al. [25] studied the fatigue behaviour of the single lap hybrid and resistance spot-welded joints. They observed that the fatigue life of hybrid joints was at least one order of magnitude higher than the just-welded specimens. Chang et al. [26] used a computational model to compare the stress distribution of resistance single lap spot-welded, bonded and hybrid spot welded-bonded joints in fatigue loading condition. They verified the computational model by performing experimental fatigue tests on the joints. It was found that the fatigue strength of the resistance spot welded-bonded joints was significantly higher than that of the welded samples, but a bit lower than the adhesively bonded joints. Lai et al. [30] studied the fatigue behaviour of single lap ultrasonic spot-welded joints with and without adhesive. They realized that the fatigue strengths of the ultrasonic spot welded-bonded and bonded joints were similar. Regarding the failure energy, Moroni et al. [18] and Yu et al. [31] found that the failure energy of the single lap hybrid joint is higher than that of the single lap bonded joint in static loading condition.

Based on most of the mentioned studies, the hybrid and adhesively bonded joints provide higher static and fatigue strength compared to the just spot-welded joints. However, there is still doubt whether the adhesive or hybrid joints offer higher static and fatigue strength.

Little research has been done on the experimental fatigue assessment of the spot welded-bonded lap shear joints. Also, the numerical fatigue simulation of the hybrid welded-adhesively joints has not been deeply investigated. In the present work, the static and fatigue mechanical behaviour of the ultrasonically spot-welded, adhesive and hybrid welded-adhesively bonded joints are numerically investigated considering experimental evidence previously gathered on these joints [32,33]. To have a better understanding of the experimental data, and to check its applicability to static and fatigue loading of non-cracked joints, the Virtual Crack Closure Technique (VCCT) was applied, and results are presented and discussed.

2. Experimental background

In this section, a brief overview is given on the experiments reported in Ref. [32] which constitute the reference for the simulations presented in the present paper. Thin sheets made of 6022-T4 aluminium alloy were selected to manufacture the spot-welded, bonded and hybrid joints. Shape and dimensions of the specimens are reported in Fig. 1. The USMW technique was used to spot weld the thin aluminium substrates. The two-components epoxy-based adhesive Loctite Hysol 9466 was used to manufacture the adhesively bonded joints. The mechanical properties of the substrates and adhesive are presented in Table 1. Regarding the production of the hybrid joints, two substrates were adhesively bonded together after surface preparation and then welded by the USMW method.

Fig. 1-a and 1-b show the shape and size of the single lap spot-welded, bonded and hybrid joints in detail, respectively. Also, Fig. 1-c displays the top view of a manufactured single lap hybrid joint.

Fig. 2 shows the experimental tensile-shear load-displacement curves for the considered different types of joints, extracted from Ref. [32]. Hybrid joints display a slightly higher maximum load and a larger displacement at failure. In Ref. [32], it was concluded that this could be explained as the result of a synergic effect of the combination of the two joining solutions. The results of the fatigue behaviour of the spot-welded and hybrid joints made of the same 6022-T4 aluminium alloy are reported in Ref. [33]. The geometry and the size of the joints are the same as those displayed in Fig. 1, but the length of the substrates is 132 mm. Fig. 3 compares the experimental P_{max}-N curves of the spot-welded and hybrid joints tested at 0.1 load ratio (i.e., $R = 0.1$). Generally, a sample

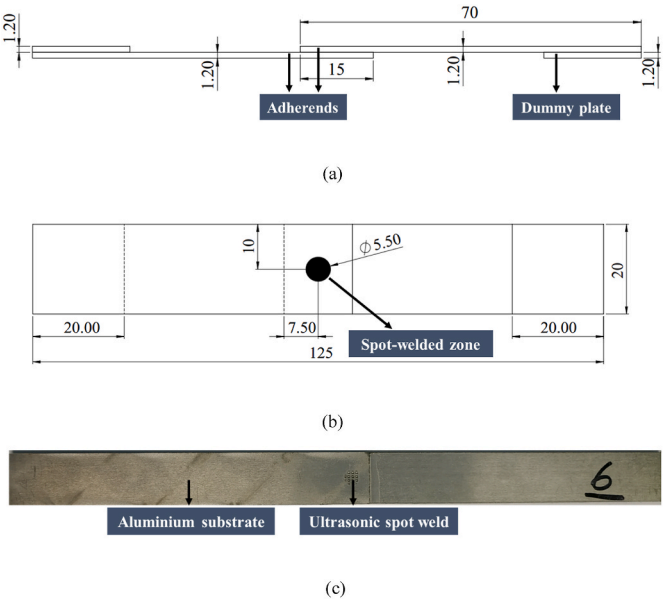

Fig. 1. a) Lateral view of the spot-welded, bonded and hybrid joints, b) top view of the spot-welded and hybrid joints, and c) top view of a typical hybrid joint (dimensions in mm, also the thickness of the adhesive layer for both bonded and hybrid joints is 0.05 mm) [32].

Table 1
Mechanical properties of the aluminium alloy and adhesive.

Material	Modulus of elasticity (GPa)	Poisson's ratio	Ultimate Strength (MPa)
6022-T4 [32]	67.20	0.30	264
Hysol 9466 [34]	1.72	0.35	32

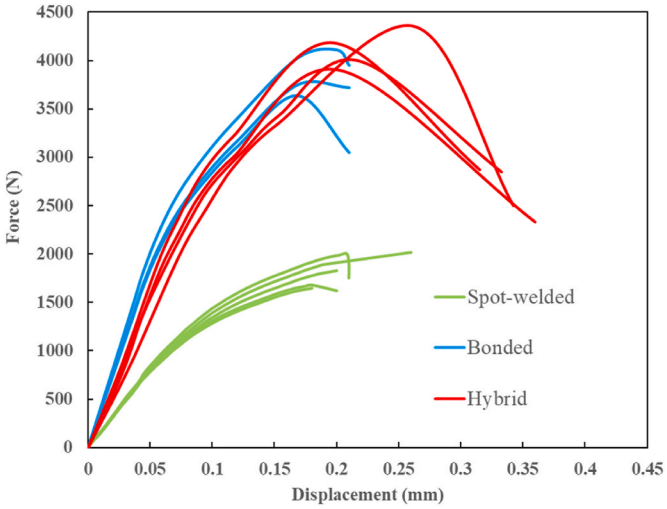

Fig. 2. The tensile-shear load-displacement experimental curves [32].

was considered fractured when the displacement of the mobile cross head of the testing machine increased by 0.5 mm with respect to the initial position at the maximum load [33]. The run-out test was assumed at 5×10^6 cycles.

In the experimental investigation reported in Refs. [7,33], two fundamental types of the failure modes were observed for the spot-welded joints at $R = 0.1$. For joints exposed to high-load levels, failure happened through the spot-welded nugget. At lower load levels,

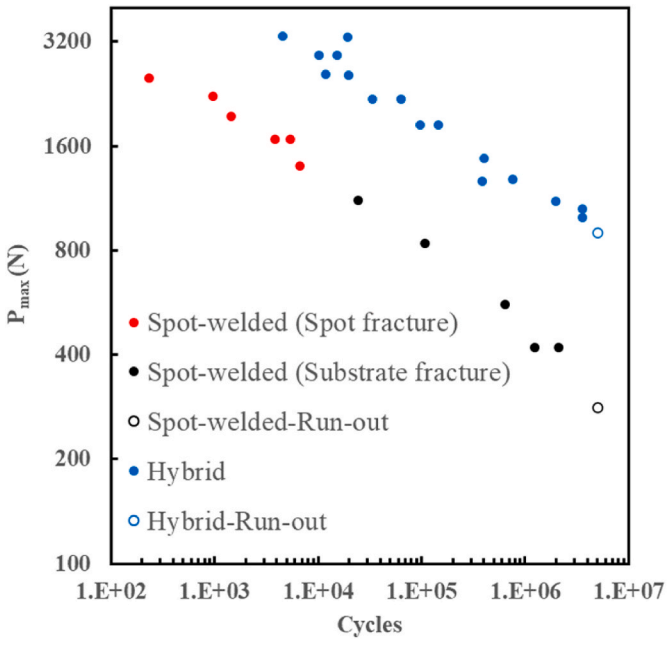

Fig. 3. Experimental fatigue P_{max}-N curves of the spot-welded with two failure mechanisms and hybrid joints at $R = 0.1$ [7,33].

the crack initiated at the weld's boundary, and then propagated through the substrate. Fig. 3 distinguishes high and low load levels at which the two failure mechanisms were observed for the spot-welded joints.

3. Finite element analysis

3.1. Static analysis

A 3-D finite element analysis utilizing Abaqus software package v. 2021 [35] was first performed to investigate numerically the static behaviour of the spot-welded, adhesively bonded and hybrid joints. The VCCT was used to estimate the static maximum loads of these joints. This technique is based on the idea that when a crack extends by a certain length δa, the released strain energy is equal to the work required to close the same crack by the same amount δa [36]. In a finite element mode, this work can be computed without actually extending the crack (hence the term virtual), but simply by multiplying the nodal forces at the crack tip by the corresponding relative nodal displacements ahead of the crack tip.

To model the considered joints, the geometry of the specimens depicted schematically in Fig. 1 was used. It is to be pointed out that the adhesive thickness was not taken into account and a zero-thickness method was employed. The Young's modulus and Poisson's ratio of the adherends are those reported in Table 1. The plastic properties were extracted from the data reported in Ref. [37].

The finite element software employs the BK (Benzeggagh-Kenane) law [38], described in Equation (1), to compute the fracture toughness of the spot-welded, adhesively bonded and hybrid joints based on the local mode-mixity:

$$G_c = G_{Ic} + (G_{IIc} - G_{Ic})\left(\frac{G_{II} + G_{III}}{G_I + G_{II} + G_{III}}\right)^{\eta} \quad (1)$$

where G_I, G_{II}, and G_{III} are the mode *I*, mode *II*, mode *III* strain energy release rates, respectively, G_c, G_{Ic}, G_{IIc} and G_{IIIc} are the fracture energies in mode *I*, mode *II* and mode *III* respectively, and η is a fitting parameter. The mode *I*, mode *II* and mode *III* fracture energy of the spot weld and adhesive materials are listed in Table 2. They were iteratively obtained by matching the experimental and numerical results as this method was already used in the literature [32,39] for an ultrasonic spot-welded joint.

Table 2
VCCT parameters of the spot weld and the adhesive.

Material	G_{Ic} (N/mm)	G_{IIc} (N/mm)	G_{IIIc} (N/mm)	η
Spot weld	0.60	1.15	1.15	1
Hysol 9466 [34]	0.44	0.68	0.68	1

A mesh size of 0.5 × 0.25 mm for each substrate of all three types of the joints was selected after a convergence analysis. Also, finer elements with a mesh size of 0.25 × 0.25 mm were used at the bonding surface. It should be noted that for the substrates, first order 3D structured elements with reduced integration (i.e., C3D8R) were adopted. Abaqus simulations adopting VCCT require the definition of a set of bonded nodes. Fig. 4-b to 4-d present the top view of the selected bonded nodes, and showcases the location of connection (i.e., red nodes) for the spot-welded, adhesively bonded and hybrid joints. Also, a pre-crack must be specified to apply VCCT. So, a fictitious pre-crack was inserted, although the initial state of the joints had no crack as the same was done in the literature [40,41] for a Single Lap Joint. The unbonded nodes that are needed to act as a pre-crack in the spot-welded, adhesively bonded and hybrid joints to allow crack propagation are depicted in Fig. 4-b to 4-d.

Considering the boundary conditions, two reference points (RPs) were defined (i.e., red points in Fig. 4-a) and coupled to the left and right sides of the samples as shown in Fig. 4-a. Then, 1 mm displacement was applied to the RP on the right side and all displacements and rotations of the RP on the left were constrained.

3.2. Fatigue analysis

To study numerically the fatigue behaviour of SLJ specimens, a 3-D finite element analysis was performed using VCCT. The fatigue crack growth simulation capability is provided in Abaqus using a very specific procedure, called Direct Cyclic (DC) method [35]. According to the Abaqus manual [35], fatigue crack initiation occurs if Equation (2) is fulfilled. Crack propagation is then started and the number of cycles ΔN required to extend the crack is obtained from Equation (3) (i.e., Paris-like equation):

$$\frac{N}{C_1 \Delta G^{C_2}} \geq 1 \quad (2)$$

$$\frac{da}{dN} = C_3 \Delta G^{C_4} \quad (3)$$

where N is the elapsed number of cycles, C_1 and C_2 are input coefficients, $\Delta G = G_{max} - G_{min}$ is the difference between maximum and minimum strain energy release rate, a is the crack length and C_3 and C_4 are Paris law parameters. As is common in the literature [36], C_1 and C_2 of both the spot weld and the adhesive were chosen so that crack propagation happens instantly. Coefficients C_3 and C_4 of the adhesive were adapted from Ref. [42] at $R = 0.1$. Parameters C_3 and C_4 of the spot weld were not available in the literature, therefore these parameters were obtained by fitting the experimental data of the spot-welded joint, as it will be discussed in Section 4.2 in detail. Table 3 lists the adopted input coefficients related to the crack initiation (i.e., C_1 and C_2) and Paris-like parameters (i.e., C_3 and C_4) of both the spot weld and the adhesive materials.

The values of the C_j parameters are sensitive to the mode mixity. However, the fatigue simulation algorithm implemented in Abaqus using VCCT in a Direct Cyclic (DC) step adopted in this work can use only one set of constant parameters throughout the entire simulation and cannot take into account the variation of the mode mixity as the crack propagates. Future works should address this point.

The mesh of the samples, the size and type of the elements were the same as those used for the static case. To specify the time increment in

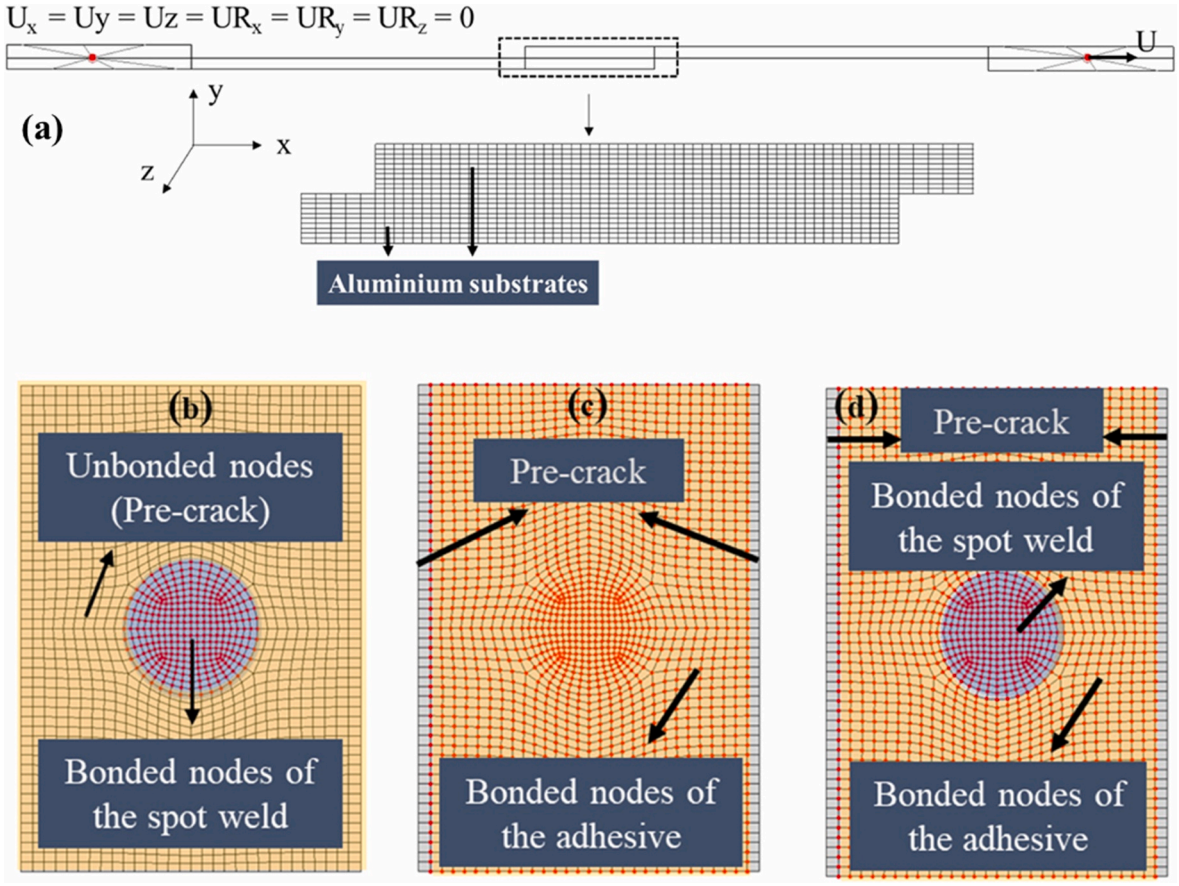

Fig. 4. a) Boundary conditions, element shape, and up view of the surface connections for the b) spot-welded, c) adhesively bonded and d) hybrid joints.

Table 3
Fatigue properties of the spot weld and adhesive at $R = 0.1$

Material	C_1 [N/mm•cycle]	C_2 [-]	C_3 [mm^2/N•cycle]	C_4 [-]
Spot weld	0.0055	−0.06	4.5×10^{-11}	3.00
Hysol 9466 [42]	0.0035	−0.01	7.4×10^{-10}	3.13

the fatigue simulations, a convergence analysis was performed. Finally, 100-time integration points were employed with an initial time increment of 0.01.

4. Results and discussion

4.1. Numerical static results

To model crack propagation in the bonded joint under static loading, four different fictitious pre-crack sizes including 0.1, 0.25, 0.5 and 1 mm at both sides of the specimen were considered (Fig. 4-c). Fig. 5 compares the experimental load-displacement curves with those obtained by numerical simulations assuming different pre-crack sizes. According to the results, there is better agreement between the experimental data and numerical results with 0.1- and 0.25-mm pre-crack sizes. To decrease the computational time, 0.25 mm was considered for the fictitious pre-crack size of both bonded and hybrid joints.

The load-displacement curves of the spot-welded, bonded and hybrid joints obtained from the numerical results have been compared with the experimental tests in Fig. 6. The comparison between the mean experimental fracture loads and stiffnesses and those obtained from numerical simulations was reported in Table 4. According to Table 4, the experimental and numerical outcomes are reasonably similar. The bonded joint has the greatest difference between the mean experimental data

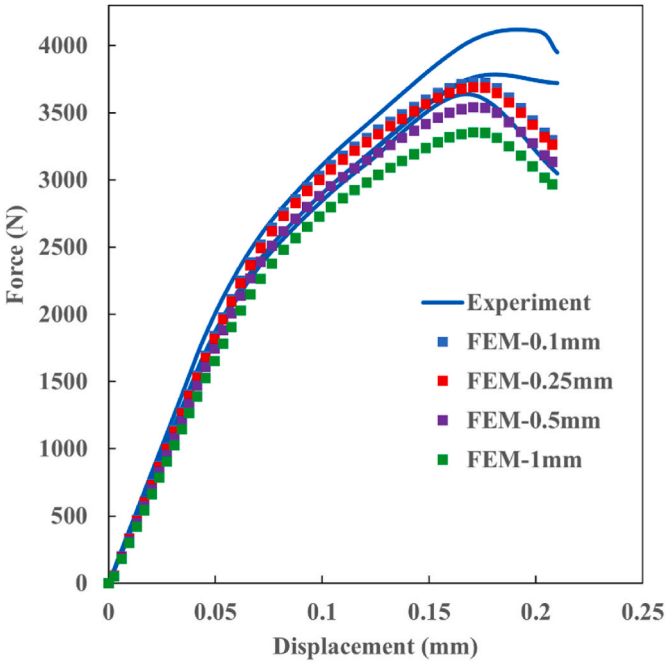

Fig. 5. Comparison of experimental load-displacement curves and numerical ones using VCCT modelling with different fictitious pre-crack sizes for the bonded joint.

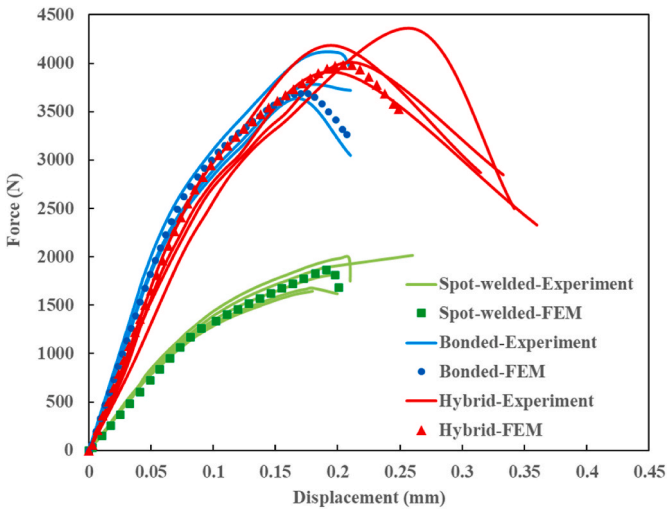

Fig. 6. Load-displacement graphs from VCCT modelling: comparison to the experimental data for three kinds of the SLJs.

and numerical results, with 7.4 and 3.6 % differences for the stiffness and fracture load, respectively. As a results, VCCT simulations using the fracture energies mentioned in Table 2 can accurately reflect the static response of these joints.

Fig. 6 shows that the weakest and most compliant one is the spot-welded joint, while the bonded and hybrid joints seem to be stiffer and stronger. This is likely due to their continuous bond area, compared to the reduced contact of the spot-welded joint. In other words, for the spot-welded joints, only the welded region at the overlap is subjected to the applied load, as compared to the full overlap area in the case of the bonded and hybrid joints. Additionally, the spot weld is mostly exposed to shear damage in the spot-welded joints [31], because there are high stress concentrations surrounding the nugget. However, lower stress concentrations happened at the edges for the bonded and the hybrid joints, as it was reported in Ref. [31].

Based on the results of Table 4, it can be observed that the numerical static strength of the hybrid joint is slightly higher than that of the bonded joint. Considering the experimental data, the p-value with *t*-test was calculated to determine if there is statistically significant relationship between the experimental static strength of the bonded and the hybrid joints. The p-value between fracture loads of the bonded and hybrid joints is 0.16. Therefore, the experimental fracture loads for both the bonded and the hybrid joints are not statistically different enough to suggest a better static strength of the hybrid joint compared to the bonded one.

It is still debated whether bonded or hybrid joints give greater static strength. For example, authors in Ref. [18] concluded that hybrid joint provide better static strength with respect to the bonded joint. However, in another research [31], the static strength of the hybrid joint was lower than that of the bonded joint, because the stress distribution of the bonded joint was more uniform than that of the hybrid joint.

4.2. Numerical fatigue results

Fatigue tests were simulated by VCCT Direct cyclic steps in Abaqus, where the same loads levels applied during the experiments were defined. Moreover, the fatigue behaviour of the bonded joints was simulated under the same loads (no tests were conducted on simply adhesively bonded joints). According to the experimental procedure, a joint was considered broken once the displacement of the point where the load is applied was increased by 0.5 mm with respect to the initial position in the numerical fatigue simulations. The Paris-like parameters of the spot weld material were iteratively obtained using numerical simulations. The numerical data were compared to the experimental results of the spot-welded joint at which failure happened at the nugget zone (i.e., red dots in Fig. 3). Based on Fig. 7, the numerical P_{max}-N curve is between the lower and upper bond of the experimental data with a 95% confidence interval obtained by instructions reported in ASTM E739-10 standard [43]. The considered parameters listed in Table 3 were thus able to capture the fatigue behaviour of the spot-welded joint.

Fig. 8 displays the experimental P_{max}-N graph of the hybrid joints and the numerical results for both bonded and hybrid joints obtained from VCCT modelling at $R = 0.1$. Also, Fig. 8 shows the 95% confidence analysis for the experimental results of the hybrid joints obtained using ASTM E739-10 standard [43]. It is seen that the numerical results obtained by VCCT modelling and Direct Cyclic method agree with the experimental data for hybrid joints at $R = 0.1$. According to Fig. 8, numerical results show better agreement with the experimental data in the middle section of the curve. This could potentially be attributed to the effect of the load level on Paris-like parameters (i.e., C_3 and C_4). Since these parameters were assumed to be unchanged for each load level at the same load ratio (R), a better agreement is just observed in the middle of the curve compared with the upper and lower part of the curve. This phenomenon was reported in the literature [44,45]. Additionally, it can be found from comparison between Figs. 7 and 8, the hybrid joint has considerably superior fatigue performance than the

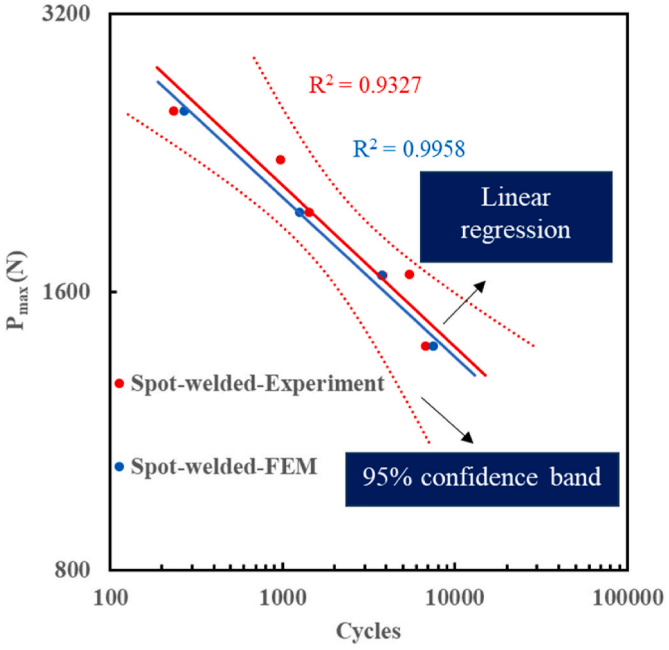

Fig. 7. P_{max}-N curve from VCCT modelling compared to the experimental data for the spot-welded joint at $R = 0.1$.

Table 4
The mean fracture loads and stiffnesses for SLJs with different joining methods.

Type of joint	Mean experimental fracture load (N)	Numerical fracture load (N)	Mean experimental stiffness (N/mm)	Numerical stiffness (N/mm)
Spot-welded	1828 ± 180	1865	15972 ± 59	15267
Bonded	3823 ± 251	3690	37659 ± 220	35076
Hybrid	4107 ± 199	3985	31036 ± 2864	32916

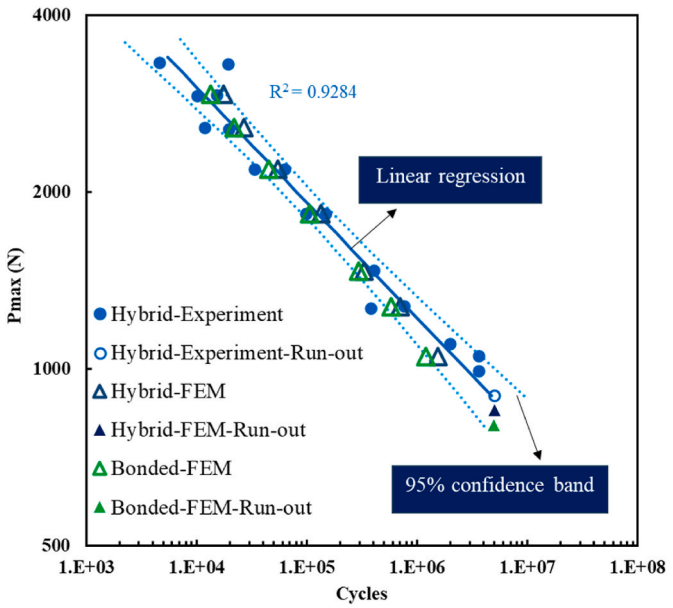

Fig. 8. P_{max}-N data from VCCT modelling compared to the experimental results for hybrid joint at $R = 0.1$.

spot-welded one. This is probably because the fatigue performance reflects the static superiority of the hybrid joints.

Moreover, from a statistical point of view, the numerical P_{max}-N curves of the bonded and hybrid joints presented in Fig. 8 are indistinguishable. This is confirmed by focusing more on the numerical outcomes discussed in the following.

According to the numerical observations displayed in Fig. 9, the mode *I* and mode *II* strain energy release rate (i.e., G_I and G_{II}, respectively) of the spot weld is very low compared to the adhesive until the crack reaches the spot-welded area (Fig. 9-a and 9-b). Therefore, for the initial phase of the fatigue life, the spot-welded zone is thus not loaded under the fatigue loading and the adhesive plays the major role in sustaining the applied load. This justifies the similarity of the fatigue behaviour of the bonded and hybrid joints. However, once the crack reaches the spot-welded zone, the strain energy release rate of the spot-welded area becomes not negligible (Fig. 9-c and 9-d).

4.2.1. *Effect of load ratio*

In this section, the fatigue behaviour of the hybrid joints at different load ratios is studied. Fig. 10 presents the fatigue experimental results for the hybrid joints at two different load ratios [33]. As it was reported in the literature [44,46], Paris law coefficients (i.e., C_3 and C_4 in Equation (3)) change according to testing condition, such as load ratio. Allegri et al. [47] proposed a relation to consider the effect of load ratio on mode *II* delamination growth of fiber reinforced epoxies. If this relation is rewritten according to ΔG in order to be used with Direct Cyclic method (i.e., Equation (3)), it will lead to various slopes (i.e., *C4*) for different load ratios, while Fig. 10 shows similar slope for hybrid joints at both 0.1 and 0.3 load ratios. Therefore, Allegri's model cannot be used in this study to model the hybrid joints with different load ratios. Also, Rocha et al. [44] studied the mode *I* fatigue crack growth of the bonded joints with different load ratios using a new relation suggested by Ref. [48] for metals. However, it is impossible to reformulate it to obtain an equivalent ΔG, as required by the VCCT algorithm implemented in the Abaqus software.

In Fig. 10, the number of cycles to failure is reported as a function ΔP. First, it can be observed that the trend of the data for 0.1 and 0.3 load ratios fallow a linear relationship with nearly the same slope (i.e., C_4). Second, the data series of the two load ratios are characterized by having the same number of cycles for the same ΔP. Based on these

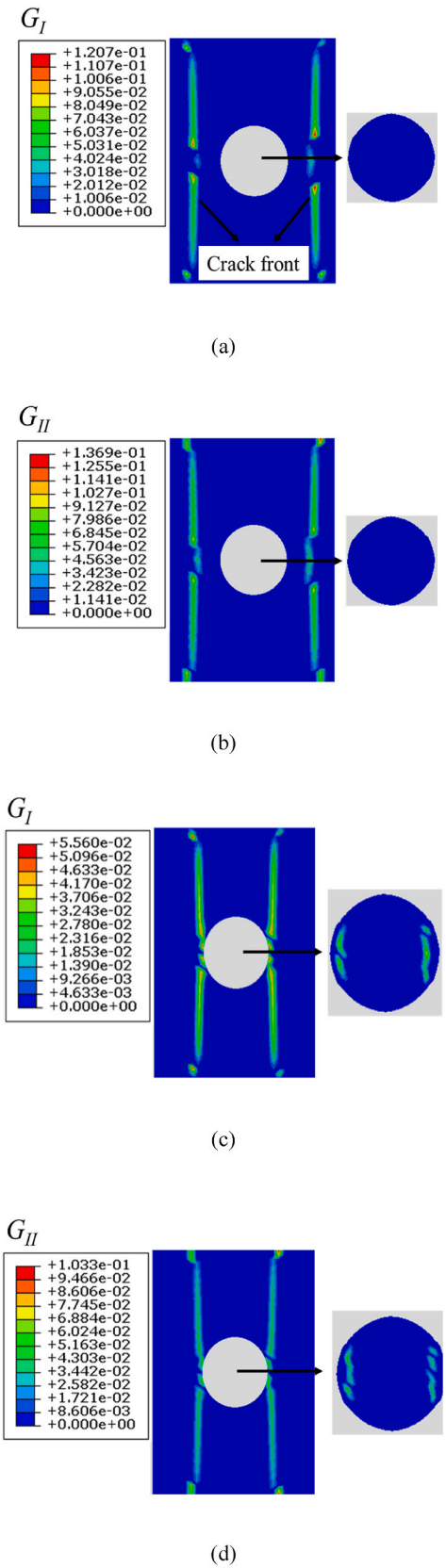

Fig. 9. The distribution of a) mode *I* and b) mode *II* strain energy release rate at 142300 cycles, and c) mode *I* and d) mode *II* strain energy release rate at 256420 cycles for a hybrid joint with 1470 N maximum load.

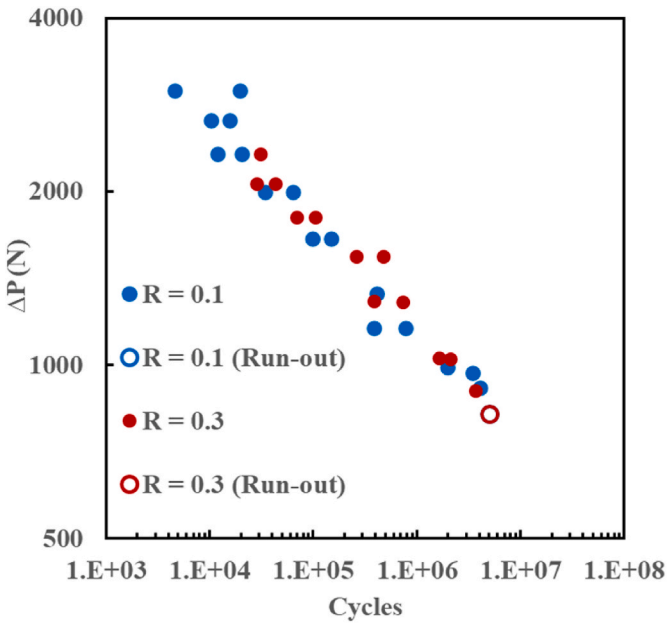

Fig. 10. Fatigue ΔP – N curves for hybrid joints at different load ratios [33].

observations, the Paris law parameters can be inferred for $R = 0.3$.

Equation (4) shows the general relationship between the strain energy release rate and the load ratio [49]. Also, the relationship between strain energy rate and the stress intensity factor (K) has been presented in Equation (5).

$$\Delta G = G_{\max}\left(1 - R^2\right) \tag{4}$$

$$G_{\max} = \frac{K_{\max}^2}{E} = \frac{\sigma^2 Y^2 \pi a}{E} = \frac{{P_{\max}}^2 Y^2 \pi a}{A^2 E} \tag{5}$$

where E is the Young modulus, σ is the stress, Y is the shape function, a is crack length, and P and A are applied load and cross section, respectively. The term $\frac{Y^2 \pi a}{A^2 E}$, is considered as a constant value named, k. So, Equation (4) can be described as follows:

$$\Delta G = kP_{\max}^2\left(1 - R^2\right) \tag{6}$$

Since the maximum load is given by $P_{\max} = \frac{\Delta P}{1-R}$, hence Equation (6) is rewritten as follows:

$$\Delta G = \frac{k\Delta P^2(1+R)}{1-R} \tag{7}$$

Given that the fatigue crack growth rates for $R_1 = 0.1$ and $R_2 = 0.3$ are almost the same for the same applied ΔP, the Paris law relation (i.e., Equation (3)) for these two load ratios with the same slope can be written as follows, by equating the crack growth rates:

$$C_3\left[\left(\frac{1+R_1}{1-R_1}\right)k\Delta P^2\right]^{C_4} = C_3'\left[\left(\frac{1+R_2}{1-R_2}\right)k\Delta P^2\right]^{C_4} \tag{8}$$

where C_3' is Paris parameter corresponds to $R_2 = 0.3$. Considering that k is constant; so, Equation (8) is simplified as follows:

$$C_3\left[\left(\frac{1+R_1}{1-R_1}\right)\right]^{C_4} = C_3'\left[\left(\frac{1+R_2}{1-R_2}\right)\right]^{C_4} \tag{9}$$

The values of C_3 and C_4 for the spot weld and adhesive have been already shown in Table 3; therefore, C_3' is calculated using Equation (9). Table 5 lists the fatigue coefficients of both spot weld and adhesive used to simulate hybrid joint at $R = 0.3$. The values considered for the crack initiation coefficients (i.e., C_1 and C_2) for both $R = 0.1$ and 0.3 are the same.

Table 5
Fatigue properties of the spot weld and adhesive at $R = 0.3$

Material	C_1 [N/mm•cycle]	C_2 [-]	C'_3 [mm^2/N•cycle]	C_4 [-]
Spot weld	0.0055	−0.06	1.3×10^{-11}	3.00
Hysol 9466	0.0035	−0.01	2.0×10^{-10}	3.13

The experimental and numerical results for the hybrid joints subjected to fatigue loading at $R = 0.3$ have been compared in Fig. 11. It is observed that VCCT simulations using Direct Cyclic approach and the considered fatigue properties mentioned in Table 5 can predict the fatigue strengths of the hybrid joints at $R = 0.3$. The considered method in this study to investigate the effect of the load ratio has been obtained only according to the experimental observations. Therefore, to establish if the relationship expressed by Equation (9) can be considered valid for all R ratios and loading conditions, more tests are required.

5. Conclusions

In this study, both the static and the fatigue behavior of three types of the joints including spot-welded made by USMW technique, bonded and hybrid joints were numerically investigated using VCCT. The numerical results were compared with the experimental observations. The following points can be concluded based on the acquired results:

- By VCCT, adding a fictitious initial short crack, it was possible to model both the static and the fatigue behavior of the joints with good agreement with the experimental results.
- In the static simulations, the bonded and hybrid joints were stiffer and stronger than the spot-welded joints subjected to the same static loading as seen in the experimental tests.
- The numerical static strength of the hybrid joint was slightly higher than the bonded joint, however this improvement was not statistically significant according to the experimental results.
- In agreement with the experimental results, numerical data showed that the hybrid joints had noticeably better fatigue performance compared with USMW alone at $R = 0.1$.
- Simulations suggested that the bonded joints behaved like the hybrid ones in the fatigue loading condition at $R = 0.1$.
- A relationship between the Paris law parameters and the R ratio was proposed based on the tests conducted at two different load rations ($R = 0.1$ and 0.3) and by VCCT, using Direct Cyclic method, it was possible to predict the same effect; however, more investigation is needed for other ratios and loading conditions.

Overall, this paper showed that VCCT could capture both static and

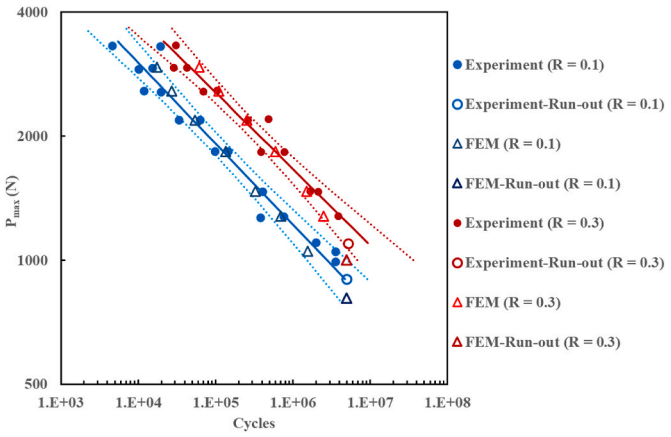

Fig. 11. P_{max}-N data from VCCT modelling compared to the experimental results for the hybrid joint at $R = 0.1$ and 0.3.

fatigue response of the spot-welded, bonded and hybrid joints, by the adoption of a fictitious, small initial crack. Also, it was numerically concluded that both bonded and hybrid joints provided similar behavior under the static and fatigue loading conditions.

Declaration of competing interest

The authors declare that they have no known competing financial interests or personal relationships that could have appeared to influence the work reported in this paper.

Data availability

Data will be made available on request.

References

[1] Wang M, Kassner M. Tensile and fatigue properties of aluminum alloy sheet 6022. J Mater Eng Perform 2002;11:166–8.
[2] Kumar S, Wu C, Kumar G, Ding W. Application of ultrasonic vibrations in welding and metal processing: a status review. J Manuf Process 2017;26:295–322.
[3] Casavola C, Pappalettere C, Tattoli F. Experimental and numerical study of static and fatigue properties of titanium alloy welded joints. Mech Mater 2009;41(3):231–43.
[4] Li J, Nie S, Kou H, Elchalakani M, Yu X, Dai G. Static and fatigue properties of 80 mm-thick Q460GJC butt weld joint. J Constr Steel Res 2021;184:106809.
[5] Amiri N, Farrahi G, Kashyzadeh K, Chizari M. Applications of ultrasonic testing and machine learning methods to predict the static & fatigue behavior of spot-welded joints. J Manuf Process 2020;52:26–34.
[6] Annoni M, Carboni M. Ultrasonic metal welding of AA 6022-T4 lap joints: Part I – technological characterisation and static mechanical behaviour. Sci Technol Weld Join 2011;16(2):107–15.
[7] Carboni M, Annoni M. Ultrasonic metal welding of AA 6022-T4 lap joints: Part II – fatigue behaviour, failure analysis and modelling. Sci Technol Weld Join 2011;16(2):116–25.
[8] da Silva L, Öchsner A, Adams R. Introduction to adhesive bonding technology. In: Handbook of adhesion technology. Springer; 2018. p. 1–7.
[9] Banea M, da Silva L. Adhesively bonded joints in composite materials: an overview. Part L: Journal of Materials: Design, and Applications 2009;223(1):1–18.
[10] Liu X, Zheng G, Luo Q, Li Q, Sun G. Fatigue behavior of carbon fibre reinforced plastic and aluminum single-lap adhesive joints after the transverse pre-impact. Int J Fatig 2021;144:105973.
[11] Zhang J, Li H, Yu H. Evaluation of multiaxial fatigue life prediction approach for adhesively bonded hollow cylinder butt-joints. Int J Fatig 2022;156:106692.
[12] Campilho R, de Moura M, Domingues J. Modelling single and double-lap repairs on composite materials. Compos Sci Technol 2005;65(13):1948–58.
[13] Campilho R, de Moura M, Domingues J, Morais J. Computational modelling of the residual strength of repaired composite laminates using a cohesive damage model. J Adhes Sci Technol 2008;22(13):1565–91.
[14] Baldan A. Adhesively-bonded joints and repairs in metallic alloys, polymers and composite materials: adhesives, adhesion theories and surface pretreatment. J Mater Sci 2004;39(1):1–49.
[15] Doyle G, Pethrick R. Environmental effects on the ageing of epoxy adhesive joints. Int J Adhesion Adhes 2009;29(1):77–90.
[16] Banea M, da Silva L, Campilho R. Temperature dependence of the fracture toughness of adhesively bonded joints. J Adhes Sci Technol 2010;24(11–12):2011–26.
[17] Yu G, Chen X, Zhang B, Pan K, Yang L. Tensile-shear mechanical behaviors of friction stir spot weld and adhesive hybrid joint: experimental and numerical study. J Met 2020;10(8):1028.
[18] Moroni F, Pirondi A, Kleiner F. Experimental analysis and comparison of the strength of simple and hybrid structural joints. Int J Adhesion Adhes 2010;30(5):367–79.
[19] da Silva L, Pirondi A, Öchsner A. Hybrid adhesive joints, vol. 6. Springer Science & Business Media; 2011.
[20] Maggiore S, Banea M, Stagnaro P, Luciano G. A review of structural adhesive joints in hybrid joining processes. Journal of Polymers (Basel) 2021;13(22).
[21] Samhan A, Darwish S. Finite element modeling of weld-bonded joints. J Mater Process Technol 2003;142(3):587–98.
[22] Santos I, Zhang W, Goncalves V, Bay N, Martins P. Weld bonding of stainless steel. Int J Mach Tool Manufact 2004;44(14):1431–9.
[23] Chang B, Shi Y, Dong S. Studies on a computational model and the stress field characteristics of weld-bonded joints for a car body steel sheet. J Mater Process Technol 2000;100(1):171–8.
[24] Campilho R, Pinto A, Banea M, da Silva L. Optimization study of hybrid spot-welded/bonded single-lap joints. Int J Adhesion Adhes 2012;37:86–95.
[25] Pizzorni M, Lertora E, Mandolfino C, Gambaro C. Experimental investigation of the static and fatigue behavior of hybrid ductile adhesive-RSWelded joints in a DP 1000 steel. Int J Adhesion Adhes 2019;95:102400.
[26] Chang B, Shi Y, Lu L. Studies on the stress distribution and fatigue behavior of weld-bonded lap shear joints. J Mater Process Technol 2001;108(3):307–13.
[27] Souza J, Aguiar R, Costa H, Reis J, Pacheco P. Numerical modelling of the mechanical behavior of hybrid joint obtained by spot welding and bonding. Compos Struct 2018;202:216–21.
[28] Costa H, Reis J, Souza J, Pacheco P, Aguiar R, Barros S. Experimental investigation of the mechanical behaviour of spot welding–adhesives joints. Compos Struct 2015;133:847–52.
[29] Sadowski T, Kneć M, Golewski P. Spot welding–adhesive joints: modelling and testing. J Adhes 2014;90(4):346–64.
[30] Lai W, Pan J. Failure mode and fatigue behavior of weld-bonded lap-shear specimens of magnesium and steel sheets. Int J Fatig 2015;75:184–97.
[31] Yu G, Chen X, Zhang B, Pan K, Yang L. Tensile-shear mechanical behaviors of friction stir spot weld and adhesive hybrid joint: experimental and numerical study. J Met 2020;10(8):1028.
[32] Moroni F, Carboni M, Pirondi A. Cohesive zone modelling of 6022-T4 aluminium alloy usmwbonded hybrid joints quasi-static failure. In: 18th European conference on fracture: fracture of materials and structures from micro to macro scale; 2010.
[33] Carboni M, Moroni F. Tensile-shear fatigue behavior of aluminum and magnesium lap-joints obtained by ultrasonic welding and adhesive bonding. Procedia Eng 2011;10:3561–6.
[34] Corbett M, McCarthy C. Numerical investigation of a hybrid mechanical-adhesive joining technology for application in lightweight composite-metal structures. 21st International Conference on Composite Materials 2017.
[35] Dassault Systemès. Abaqus 2021 manual. n.d..
[36] Krueger R. Virtual crack closure technique: history, approach, and applications. Appl Mech Rev 2004;57(2):109–43.
[37] Knezevic M, Poulin C, Zheng X, Zheng S, Beyerlein I. Strengthening of alloy AA6022-T4 by continuous bending under tension. Mater Sci Eng, A 2019;758:47–55.
[38] Benzeggagh M, Kenane M. Measurement of mixed-mode delamination fracture toughness of unidirectional glass/epoxy composites with mixed-mode bending apparatus. Compos Sci Technol 1996;56(4):439–49.
[39] Zhou B, Thouless M, Ward S. Predicting the failure of ultrasonic spot welds by pull-out from sheet metal. Int J Solid Struct 2006;43(25):7482–500.
[40] Kim M, Ri U, Hong H, Kim Y. Comparative study of failure models for prediction of mixed-mode failure characteristics in composite adhesively bonded joint with brittle/Quai-brittle adhesive using finite element analysis. Int J Adhesion Adhes 2021;109:102911.
[41] Sadeghi M, Gabener A, Zimmermann J, Saravana K, Weiland J, Reisgen U, Schroeder K. Failure load prediction of adhesively bonded single lap joints by using various FEM techniques. Int J Adhesion Adhes 2020;97:102493.
[42] Pirondi A, Moroni F. An investigation of fatigue failure prediction of adhesively bonded metal/metal joints. Int J Adhesion Adhes 2009;29(8):796–805.
[43] ASTM E739-10. Standard practice for statistical analysis of linear or linearized stress-life (S-N) and strain-life (ε-N) fatigue data. 2015.
[44] Rocha A, Akhavan-Safar A, Carbas R, Marques E, Goyal R, Ei-Zein M, Da Silva LFM. Paris law relations for an epoxy-based adhesive. Proc Inst Mech Eng Part L 2019;234(2):291–9.
[45] Monteiro J, Akhavan-Safar A, Carbas R, Marques E, Goyal R, Ei-Zein M, Da Silva LFM. Influence of mode mixity and loading conditions on the fatigue crack growth behaviour of an epoxy adhesive. 46 2020;43(2):308–16.
[46] Pirondi A, Nicoletto G. Fatigue crack growth in bonded DCB specimens. Eng Fract Mech 2004;71(4):859–71.
[47] Allegri G, Jones M, Wisnom M, Hallett S. A new semi-empirical model for stress ratio effect on mode II fatigue delamination growth. Compos Appl Sci Manuf 2011;42(7):733–40.
[48] Jones R, Hu W, Kinloch A. A convenient way to represent fatigue crack growth in structural adhesives. Fatig Fract Eng Mater Struct 2015;38(4):379–91.
[49] Wilkins D, Eisenmann J, Camin R, Margolis W, Benson R. Characterizing delamination growth in graphite-epoxy 1982;775(91982):168.